A Helical Turn Motif in Mss4 Is a Critical Determinant of Rab Binding and Nucleotide Release†

Zhongyuan Zhu, John J. Dumas, Susan E. Lietzke, and David G. Lambright*

Program in Molecular Medicine and Department of Biochemistry & Molecular Pharmacology, University of Massachusetts Medical School, Worcester, Massachusetts 01605

Received November 22, 2000

ABSTRACT: Monomeric Rab GTPases function as ubiquitous regulators of intracellular membrane trafficking. Mss4, an evolutionarily conserved Rab accessory factor, promotes nucleotide release from exocytic but not endocytic Rab GTPases. Here we describe the results of a high-resolution crystallographic and mutational analysis of Mss4. The 1.65 Å crystal structure of Mss4 reveals a network of direct and water-mediated interactions that stabilize a partially exposed structural subdomain derived from four highly conserved but nonconsecutive sequence elements. The conserved subdomain contains the invariant cysteine residues required for Zn^{2+} binding as well as the residues implicated in the interaction with Rab GTPases. A strictly conserved DΦΦ motif, consisting of an invariant aspartic acid residue (Asp 73) followed by two bulky hydrophobic residues (Met 74 and Phe 75), encodes a prominently exposed 3_{10} helical turn in which the backbone is well-ordered but the side chains of the conserved residues are highly exposed and do not engage in intramolecular interactions. Substitution of any of these residues with alanine dramatically impairs nucleotide release activity toward Rab3A, indicating that the DΦΦ motif is a critical element of the Rab interaction epitope. In particular, mutation of Phe 75 results in a defect as severe as that observed for mutation of Asp 96, which is located near the zinc binding site at the opposite end of the conserved subdomain. Despite severe defects, however, none of the mutant proteins is catalytically dead. Taken together, the results suggest a concerted mechanism in which distal elements of the conserved Rab interaction epitope cooperatively facilitate nucleotide release.

Rab GTPases comprise a large family with more than 50 members regulating discrete steps in exocytic and endocytic trafficking pathways (*1*−*3*). Like other guanine nucleotide binding proteins of the Ras superfamily, Rab GTPases cycle between active (GTP-bound)[1] and inactive (GDP-bound) forms. As the intrinsic rates of nucleotide exchange and GTP hydrolysis are slow, interconversion between these forms depends on interactions with accessory proteins. Activation is tightly regulated by exchange factors (GEFs), which promote exchange of GTP for GDP in response to extracellular or intracellular signals (*4*, *5*). Inactivation is regulated by GTPase-activating proteins (GAPs), which stimulate the hydrolysis of GTP (*6*, *7*).

Although GTPases have a similar core fold (*8*−*15*), GEFs share little or no structural homology. Crystallographic, mutational, and kinetic studies of three complexes between GEFs and the nucleotide free forms of monomeric GTPases reveal critical similarities as well as differences in the underlying mechanisms of action. The bacterial exchange factor EF-Ts utilizes a 3_{10} helical turn (residues ^{80}DFV^{82}) to displace the switch II region of EF-Tu and thereby disrupt Mg^{2+} coordination (*16*). The structural changes in the Mg^{2+} binding site act in concert with other induced conformational changes involving the P-loop as well as regions that contact the guanine base. Disruption of the P-loop and Mg^{2+} binding site also plays a key role in the crystal structures of the exchange domains of mammalian Sos (Son of Sevenless) and the yeast Sec7 protein bound to the nucleotide free forms of Ras and Arf1, respectively (*17*, *18*). In all three cases, critical interactions with the switch regions and/or P-loop are mediated by acidic and hydrophobic residues in the GEFs. However, the structures of the EF-Ts, Sos, and Sec7 exchange domains are unrelated as are the detailed interactions leading to (and conformational changes resulting from) disruption of the P-loop and Mg^{2+} binding site.

GEFs specific for one or more Rab GTPases have been identified and partially characterized. These include Rab3 GEF, which selectively recognizes Rab3 isoforms (*19*); Vps9, a yeast GEF specific for the Rab5 homologue Vps21 (*20*); p532, a large protein containing an RLD1 domain that can stimulate release of GDP from both Rab3a and Rab5 (*21*); and Rabex, a Rab5 specific GEF that contains a domain that is homologous to Vps9 (*22*). Dss4 (dominant suppressor of

† This work was supported by National Institutes of Health Grant GM 56324. D.G.L. is a Leukemia and Lymphoma Society Scholar, and J.J.D. is a NIH postdoctoral fellow.

* To whom correspondence should be addressed: Program in Molecular Medicine, Two Biotech, 373 Plantation St., Worcester, MA 01605. Telephone: (508) 856-6876. Fax: (508) 856-4289. E-mail: David.Lambright@umassmed.edu.

[1] Abbreviations: DTT, dithiothreitol; GAP, GTPase activating protein; GDP, guanosine diphosphate; GTP, guanosine triphosphate; GEF, guanine nucleotide exchange factor; EDTA, ethylenediaminetetraacetic acid; Hepes, 4-(2-hydroxyethyl)piperazine-1-ethanesulfonic acid; mant-GDP, 2′(3′)-bis-*O*-(*N*-methylanthraniloyl)GDP; NMR, nuclear magnetic resonance; OAc, acetate; PCR, polymerase chain reaction; PAGE, polyacrylamine gel electrophoresis; PEG, polyethylene glycol; P-loop, phosphate binding loop; SDS, sodium dodecyl sulfate; Tris, tris(hydroxymethyl)aminoethane.

10.1021/bi002680o CCC: $20.00
Published on Web 02/08/2001

Sec4) was identified as a spontaneous suppressor of temperature sensitive, secretory defects in Sec4, a yeast Rab required for vesicle transport from the Golgi to the plasma membrane (*23*). In vitro, Dss4 stimulates the dissociation of guanine nucleotides from Sec4. Although not lethal, disruption of the dss4 gene sharply lowers the growth rate of cells with impaired Sec4 function. Mss4, a mammalian homologue of Dss4, was cloned from a rat brain DNA library on the basis of its ability to suppress Sec4 defects (*24*). Mss4 coimmunoprecipitates with Rab3a in rat brain extracts, exhibits selective GDP release activity for exocytic Rab GTPases (Rab1, Rab3a, Rab8, and Rab10, Sec4, and Ypt1) but not endocytic Rab GTPases (Rab2, Rab4, Rab5, Rab6, Rab9, and Rab11), and facilitates neurotransmitter release when injected into squid giant nerve termini (*25*). Moreover, Mss4 is overexpressed at high levels in pancreatic and other human tumors, suggesting a possible aberrant function with respect to tumor maintenance and proliferation (*26*).

The sequences of the known Rab GEFs are diverse and exhibit no apparent homology with the exchange domains of GEFs for other GTPase families. With the exception of Mss4, little is known regarding the structure of Rab GEFs, the determinants for recognition of Rab GTPases, or the mechanism of facilitated nucleotide release. The NMR structure of human Mss4 revealed a mostly β fold stabilized by a Zn^{2+} ion coordinated by cysteine residues from two CxxC motifs (*27*). Chemical shift perturbations in the presence of Sec4 and a limited number of partially characterized site specific mutations provide an approximation of the epitope for interaction with Rab GTPases. In particular, substitution of Asp 96 with histidine disrupts Rab binding and exchange activity (*25*, *27*−*29*). However, interpretation of the effects of this mutation is complicated by the observation of an intramolecular interaction between Asp 96 and Asn 79 in the NMR model (*27*). Moreover, the role of other conserved residues with respect to Rab interaction and the nucleotide release mechanism remains to be determined.

Here we describe the 1.65 Å crystal structure of Mss4 and the results of a structure-based mutational analysis. The high-resolution structure reveals a network of direct and water-mediated interactions that stabilize a structural subdomain encoded by four evolutionarily conserved sequence regions. The conserved regions encompass two invariant CX_nC motifs as well as the known Rab interaction epitope. Although the fold is similar to that of the NMR structure, significant differences are evident throughout the protein and have functional consequences with respect to the intramolecular interactions that stabilize conserved structural elements implicated in the interaction with Rab GTPases. A detailed kinetic study of six conserved residues spanning the putative Rab interaction surface shows that both Asp 96 and conserved residues in a DΦΦ helical turn motif (residues ^{73}DMF^{75}) are critical determinants of a concerted nucleotide release mechanism reminiscent of other GEF−GTPase systems.

MATERIALS AND METHODS

Constructs and Site Specific Mutagenesis. Constructs of rat Mss4 (residues 9−123) and rat Rab3A (residues 14−186) were amplified by PCR, digested with *Bam*HI and *Sal*I, and subcloned into modified pET15 vectors containing an N-terminal six-His or ten-His tag followed by a thrombin cleavage site. The Mss4 construct eliminates an N-terminal hypervariable extension that is highly sensitive to proteolysis (D. G. Lambright, unpublished results) and poorly ordered in the NMR structure (*29*). The Rab3A construct corresponds to the GTPase domain and lacks the N- and C-terminal hypervariable regions. Hereafter, these constructs will be termed Mss4 and Rab3A for simplicity. Mutations in Mss4 were generated by overlap PCR using oligonucleotide primers containing the appropriate nucleotide substitutions. Overlapping fragments containing the substitutions were generated by PCR, gel purified, and combined in a second round of PCR with oligonucleotide primers flanking the intact coding sequences. The resulting fragments containing the desired mutation were digested with *Bam*HI and *Sal*I and subcloned into a modified pET15b vector containing an N-terminal ten-His tag followed by a thrombin cleavage site.

Expression and Purification. Mss4 and Rab3a constructs were expressed in *Escherichia coli* using modified pET15b vectors. BL21(DE3) cells harboring the modified pET15b plasmid containing Mss4 or Rab3A constructs were grown at 37 °C in 6 L of 2× YT medium, induced at an OD_{600} of 0.6 by addition of 1 mM IPTG, and harvested after 4 h at 28 °C. The cells were resuspended in lysis buffer [50 mM Tris (pH 8.0) and 0.1% mercaptoethanol], disrupted by sonication, centrifuged at 35000*g* for 1 h, and the supernatant loaded onto a Ni−NTA−agrose column (Qiagen). After washing with 10 column volumes of wash buffer [50 mM Tris (pH 8.0), 500 mM NaCl, 10 mM imidazole, and 0.1% mercaptoethanol], the fusion protein was eluted with a gradient of 10 to 150 mM imidazole (six-His tag) or 10 to 500 mM imidazole (ten-His tag) in elution buffer [50 mM Tris (pH 8.0), 100 mM NaCl, and 0.1% mercaptoethanol]. For kinetic studies, ten-His wild type and mutant Mss4 proteins were exchanged into storage buffer [10 mM Tris (pH 8.0) and 0.1% mercaptoethanol] and used without further purification. For Rab3A and for crystallographic studies with Mss4, the six-His tag was removed by incubation with a 1:2000 (w/w) ratio of thrombin (Hematologic Technologies) at 4 °C for 12 h (Rab3A) or at room temperature for 72 h (Mss4) in cleavage buffer [50 mM Tris (pH 8.0), 2 mM $CaCl_2$, and 0.1% mercaptoethanol]. Subsequent incubation with Ni−NTA−agarose eliminated any uncleaved fusion protein. Anion exchange chromatography on Resource Q (Pharmacia) followed by gel filtration on Superdex-75 (Pharmacia) yielded 30 mg (Mss4) or 90 mg (Rab3A) of >99% pure protein as judged by SDS−PAGE.

Crystallization and Data Collection. Crystals of Mss4 were grown in microseeded hanging drops containing 14% PEG-6000, 50 mM Tris (pH 8.0), 50 mM $Mg(OAc)_2$, and 10% glycerol equilibrated over an identical well solution at 4 °C. The crystals reached typical dimensions of 0.05 mm × 0.1 mm × 1 mm after 1−2 weeks. For data collection, crystals were transferred briefly to a cryosolution (30% PEG-6000 and 10% glycerol), flash-frozen in liquid propane, and maintained at 100 K in a nitrogen cryostream to minimize radiation damage. A native data set complete to 1.65 Å was collected on a Rigaku RUH3R/MAR 30 cm image plate system (see Table 1). The crystals are in the monoclinic space group $P2_1$ (a = 40.8 Å, b = 49.7 Å, c = 50.8 Å, and β = 94.8°) with two molecules in the asymmetric unit related by a noncrystallographic 2-fold screw axis. All data were processed with Denzo and scaled with Scalepack (*30*).

Table 1: Structure Determination and Refinement

Data Collection[a]

	native	$TbCl_3$
resolution (Å)	20−1.65	20−3.0
R_{sym} (%)[b]	6.5 (28.2)	5.6 (13.1)
$\langle I/\sigma \rangle$	17.1 (3.7)	16.0 (8.0)
completeness (%)	99.6 (97.2)	98.9 (95.1)
⟨redundancy⟩	3.1	2.3

SIRAS Phasing[a]

	acentric	centric
phasing power	0.91	0.72
anomalous phasing power	0.01	
figure of merit	0.25	0.45

Molecular Replacement

	molecule A	molecule B
Euler angles (Q_1, Q_2, Q_3) (deg)	282.0, 35.5, 261.8	89.9, 35.4, 274.2
fractional coordinates (x, y, z)	0.474, 0.00, 0.054	0.043, 0.875, 0.552
correlation coefficient[c]	highest peak 23.2	highest false peak 20.9

Refinement

			rms deviations	
resolution (Å)	R factor	R_{free}[d]	bond lengths (Å)	bond angles (deg)
7.0−1.65	21.4	25.6	0.013	1.9

[a] Values in parentheses represent the highest-resolution shell. [b] $R_{sym} = \Sigma_h\Sigma_j|I_j(h) - \langle I(h)\rangle|/\Sigma_h\Sigma_j I_j(h)$. [c] Values after rigid body refinement from 8 to 3.0 Å. [d] R value for a 5% subset of reflections selected at random and omitted from refinement.

Structure Determination. The structure of Mss4 was determined by a combination of single isomorphous replacement with anomalous scattering (SIRAS) and molecular replacement (MR) based on the averaged NMR model. Native crystals were soaked with various heavy atom reagents in a stabilizer solution of 35% PEG-8000, 10 mM Tris (pH 8.0), and 10% glycerol. A complete data set, including Friedel pairs, was collected for a 10 mM $TbCl_3$ derivative. Two sites were located giving rise to Harker and cross-peaks that were present in both the anomalous and isomorphous difference Patterson maps. Both sites refined to occupancies of ∼0.7 using MLPHARE and provided a phasing power of 0.91 for data in the range of 20−4.5 Å (Table 1). Solvent contrast and partial connectivity were evident in the weighted Fourier map calculated using SIRAS phases. Due to nonisomorphism, the weak SIRAS phases from the $TbCl_3$ derivative were insufficient for determining the structure. Using a search model derived from the averaged NMR structure, putative rotation function solutions were selected based on consistency with the self-rotation function and subjected to a translation search followed by rigid body refinement. Although the resulting correlation coefficients and R values yielded ambiguous results, the correct solution was identified by the following criteria: (i) good packing, (ii) correct Tb^{3+} sites obtained from isomorphous and anomalous difference Fourier maps calculated with MR phases, and (iii) agreement with the SIRAS map. Multiple rounds of simulated annealing, in which regions with poor density were omitted, followed by manual rebuilding were interleaved with gradual extension of the resolution to 1.65 Å. All computations for molecular replacement were conducted with Amore as implemented in CCP4 (*31*) and subsequent refinement with X-PLOR (*32*). Interactive model building was performed with the program O (*33*). Structural figures were generated with Molscript (*34*) or GRASP (*35*), combined with GL_Render (L. Esser), and rendered with Raster3D (*36*).

Nucleotide Release Assays. Rab3A was loaded with the fluorescent GDP analogue 2′(3′)-bis-*O*-(*N*-methylanthraniloyl)GDP (mant-GDP, Molecular Probes) (*37*) by incubating for 2 h at room temperature in loading buffer [20 mM Hepes (pH 7.5), 150 mM NaCl, and 5 mM EDTA] containing a 25-fold excess of mant-GDP. The exchange reaction mixture was transferred to ice, the reaction terminated by addition of 10 mM $MgCl_2$, and free mant-GDP removed by gel filtration on a prepacked D-Salt column (Pierce). For nucleotide release assays, Rab3A bound to mant-GDP was diluted to a concentration of 50 nM in exchange buffer [20 mM Hepes (pH 7.5), 150 mM NaCl, and 0.5 mM $MgCl_2$]. The dissociation of mant-GDP at various concentrations of Mss4 was assessed by measuring the decrease in fluorescence that accompanies release of mant-GDP in the presence of a large excess of GTP. Nucleotide release reactions were initiated by addition of GTP (1 mM final concentration) with or without varying concentrations of Mss4. Samples were excited at 360 nm, and the emission was monitored at 440 nm using an ISS spectrofluorimeter with a 1 nm band-pass on both the excitation and emission monochromators. Under the conditions used in these experiments ([Mss4] ≫ [Rab3A−mant-GDP]), the nucleotide release reaction is pseudo-first-order with respect to [Mss4] and proceeds to completion with an exponential time course. An observed pseudo-first-order rate constant (k_{obs}) was obtained by a nonlinear least-squares fit of the observed decay at each concentration of Mss4 to the exponential function

$$I(t) = (I_o - I_\infty)\exp(-k_{obs}t) + I_\infty \quad (1)$$

Apparent k_{cat} and K_m values were extracted from a nonlinear least-squares fit of the pseudo-first-order rate constants as a function of [Mss4] to the hyperbolic function

$$k_{obs} = k_{cat}[\text{Mss4}]/(K_m + [\text{Mss4}]) + k_{intr} \quad (2)$$

where k_{intr} accounts for the intrinsic rate of nucleotide release and was fixed at the measured value of 7.5×10^{-5} s^{-1}.

Although the average standard deviation in k_{obs} calculated from two to four replicate measurements is roughly 10%, the uncertainty in the estimation of K_m and k_{cat} is considerably larger due to incomplete data at high Mss4 concentrations. To obtain an error estimate that reflects the much larger uncertainty in the parameter estimation, k_{cat} (or K_m) was treated as a freely adjustable parameter while the value of the fixed parameter, K_m (or k_{cat}), was systematically incremented in both directions until χ^2 was twice that obtained when both k_{cat} and K_m were treated as freely adjustable parameters. The values of the fixed parameter at the lower and upper limits where χ^2 equals twice the fitted minimum correspond to a confidence interval of 68.3% (*38*) and were used as the limits of the estimated error range in Table 2. A similar procedure was used to determine the error range for

Table 2: Summary of Kinetic Parameters for Mss4 Mutants

protein	k_{cat}[a] ($\times 10^{-3}$ s^{-1})	error range[b]	K_m[a] ($\times 10^{-6}$ M)	error range[b]	k_{cat}/K_m[a] (M^{-1} s^{-1})	error range[b]	fold decrease in k_{cat}/K_m
wild type	7.6	6.8−8.6	11	7.5−16	690	500−970	1
S28A	5.1	4.5−6.3	35	25−68	150	110−200	4.6
D73A	13	8.5−30	245	135−700	54	45−65	13
M74A	8.4	6.5−13	200	120−390	42	35−52	16
F75A	3.9	3.4−4.8	290	230−390	13	9.9−17	53
N79A	3.3	2.7−4.2	42	28−65	79	61−105	8.7
D96A	2.7	2.1−3.6	130	85−205	21	18−25	33

[a] Best fit parameter values obtained from the data in panels C and D of Figure 5 (see Materials and Methods). [b] The error range corresponds to the 68.3% confidence interval (equivalent to one standard deviation of a normal distribution) and includes measurement error as well as uncertainty in the estimation of parameters due to parameter correlation and incomplete data at high Mss4 concentrations (see Materials and Methods).

the catalytic efficiency (k_{cat}/K_m). In this case, the data were fit to the equivalent hyperbolic equation

$$k_{obs} = (k_{cat}/K_m)[\text{Mss4}]/(1 + [\text{Mss4}]/K_m) + k_{intr} \quad (3)$$

where K_m was treated as a freely adjustable parameter while the k_{cat}/K_m ratio was systematically incremented. As would be anticipated, the relative uncertainty in k_{cat}/K_m, which corresponds to the slope of eq 2 at low Mss4 concentrations, is considerably less than the relative uncertainty in the individual parameter values. Consequently, k_{cat}/K_m provides a more reliable, though less informative, measure of the magnitude of the defects resulting from alanine substitution.

Limited Proteolysis. Wild type and mutant Mss4 proteins at a concentration of 0.1 μg/μL were incubated at 20 °C with 0.05 unit/μL endoproteinase LysC or 2 mg/mL endoproteinase ArgC in proteolysis buffer [20 mM Hepes (pH 7.5), 10% glycerol, and 2 mM DDT]. Aliquots were withdrawn at a series of time points from 0.5 to 8 h and the proteolysis reactions terminated by addition of TLCK to a final concentration of 50 μM followed by boiling in SDS sample buffer for 5 min. Samples were loaded onto an 18% SDS−polyacrylamide gel, which was subsequently stained with Coomassie Blue and digitized with a digital scanner (Afga). The relative intensity of each band on the gel was determined using a commercial software package (Image Quanta).

RESULTS

Structure Determination. Crystals of Mss4 were obtained from a deletion construct (residues 9−123) that lacked the N-terminal hypervariable region. The asymmetric unit contains two molecules related by a noncrystallographic 2-fold screw axis. Each molecule in the asymmetric unit was refined independently from 7 to 1.65 Å. The final refined model includes residues 9−123, two Zn^{2+} ions, and 182 ordered water molecules and has an *R* value of 21.4% and a free *R* value of 25.6%. The stereochemistry is excellent, and there are no main chain $\Phi-\Psi$ values outside allowed regions of the Ramachandran plot. Due to crystal contacts, the βE−βF loop is partially ordered in molecule B but disordered in molecule A, consistent with the high mobility of this region in the NMR structure (*27*).

Overall Structure and Comparison with the NMR Model. The fold of Mss4 consists of a central β sheet (βG−βK) flanked by a β hairpin (βB−βC) on one side and a small variable sheet on the other (Figure 1). The only other notable secondary structural features are two 3_{10} helical turns (3_{10}A and 3_{10}B). A single Zn^{2+} ion, coordinated by the thiol groups of cysteine residues from two CXXC motifs located in the

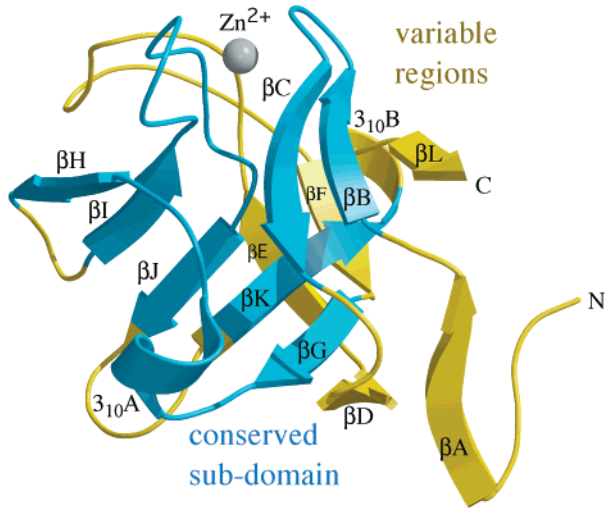

FIGURE 1: Overall structure of Mss4. Ribbon representation of the Mss4 crystal structure with conserved regions highlighted in blue, variable regions highlighted in yellow, and the Zn^{2+} ion depicted as a gray sphere.

βB−βC and βI−βJ loops, appears to play an important structural role by reinforcing the hydrophobic core formed by the βB−βC hairpin, the βG−βH loop, and the central β sheet.

Although the overall fold resembles that of the averaged NMR model (*29*), significant differences are evident throughout the protein (Figure 2A). Superposition of the NMR and crystal structures yields a rms deviation of 1.3 Å for Cα atoms. In contrast, the rms deviation for Cα atoms following superposition of the two independently refined molecules in the asymmetric unit is 0.39 Å, with much of the difference arising from the flexible βE−βF loop (Figure 2B). The significant global differences between the NMR and crystal structures are likely due to the absence of long-range order information in the NMR data and are comparable in magnitude to differences typically observed for superposition of low- and high-resolution crystal structures. These differences result in an alternative description of intramolecular interactions mediated by conserved residues and have functional consequences with respect to the structural basis for Mss4-catalyzed nucleotide release. For example, a hydrogen bond between Asp 96 and Asn 79 in the NMR model was suggested to play a structural role in stabilizing the conformation of the βG−βH loop (*29*). In the crystal structure, however, Asn 79 and Asp 96 do not interact directly but rather through a partially ordered surface water molecule. This interaction is unlikely to be a significant stabilizing factor. Instead, the side chain NH group Asn 79 donates a hydrogen bond to

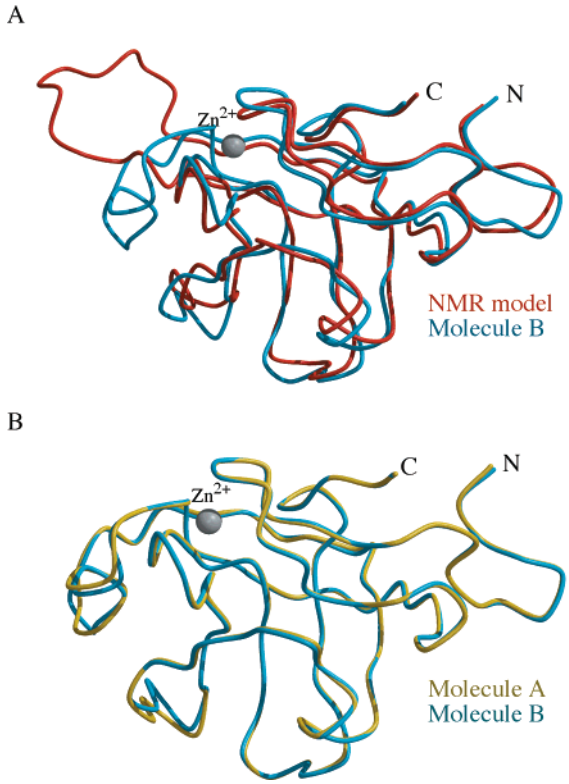

FIGURE 2: Comparison of the crystallographic and NMR models. (A) Superposition of molecule A with the averaged NMR model (*29*). (B) Superposition of the two independently refined molecules in the asymmetric unit.

the backbone carbonyl oxygen of Arg 29, whereas the carboxylate group of Asp 96 contacts the hydroxyl group of Ser 28 in the βB−βC loop, both directly and via a well-ordered, buried water molecule. The implications of these and other interactions with respect to the structural and functional properties of Mss4 are considered below.

Identification of an Evolutionarily Conserved Subdomain. A pairwise sequence alignment between mammalian Mss4 and yeast Dss4 based on the NMR structure identified two conserved regions corresponding to the βG−βH and βI−βJ hairpins (*29*). Curiously, only the second of two CXXC motifs in Mss4 was conserved in Dss4. Consequently, it was suggested that the carboxylate groups of Asp 20 and Asp 21 might serve as ligands, thus preserving the Zn^{2+} binding site (*29*). However, the detailed network of direct and water-mediated interactions that stabilize the Zn^{2+} binding site in the Mss4 crystal structure suggests an alternative alignment that is consistent with the known structural and functional properties of both Mss4 and Dss4 (Figure 3).

Using the mouse Mss4 amino acid sequence as a query, we searched the GenBank, EMBL, FlyBase, and ACEDB databases for homologous proteins (*39*, *40*). Expressed sequence tags (ESTs) for five new Mss4 homologues were identified in diverse organisms, indicative of broad evolutionary conservation. An alignment of the Mss4 sequences based on the crystal structure reveals two additional conserved regions, one corresponding to the βB−βC hairpin and the other to the βK strand. Together, the four conserved regions (CR1−CR4) encode a structural subdomain that includes the Zn^{2+} binding site, the primary hydrophobic core, and the Rab interaction epitope as defined by NMR chemical shift perturbations (*29*). A less extensive, secondary hydrophobic core formed between the conserved subdomain and the variable sheet may provide additional stability, although this feature is likely to vary considerably within the Mss4 family. CR1 and CR3 each contain a canonical CXXC motif, with the exception of Dss4 in which the first CXXC motif is substituted with a CX_4C motif. Although less common,

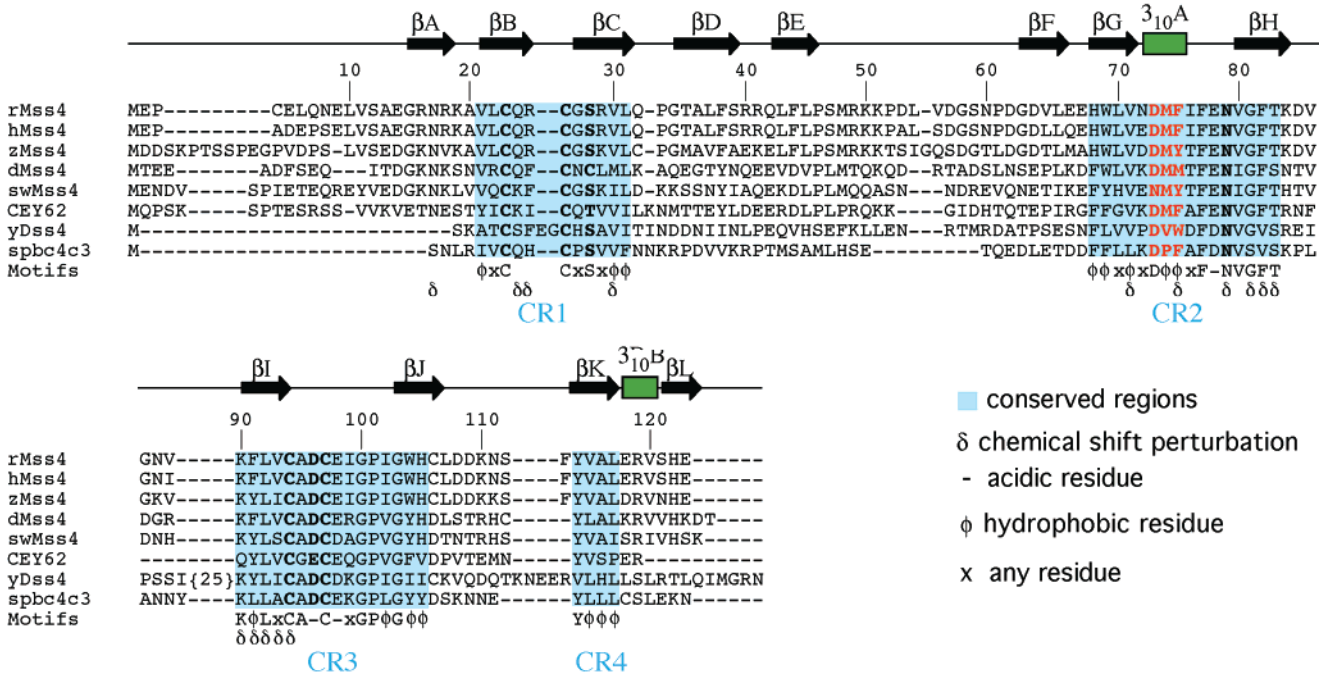

FIGURE 3: Structure-based sequence alignment of Mss4 homologues with conserved regions highlighted in blue. A "δ" below the alignment indicates residues that undergo chemical shift perturbations in the presence of Sec4 (*29*). Sequences were obtained from the following databases: mMss4, mouse (emb X70496); hMss4, human (gb L10336); zMss4, zebrafish (gb AW778533); dMss4, *Drosophila* (gb A05555); swMss4, *B. mori* (dbj AU006382); CEY62, *C. elegans* (emb CEZK970); yDss4, *S. cerevisiae* (emb X70495); and spbc4c3, *S. pombe* (emb AL021730).

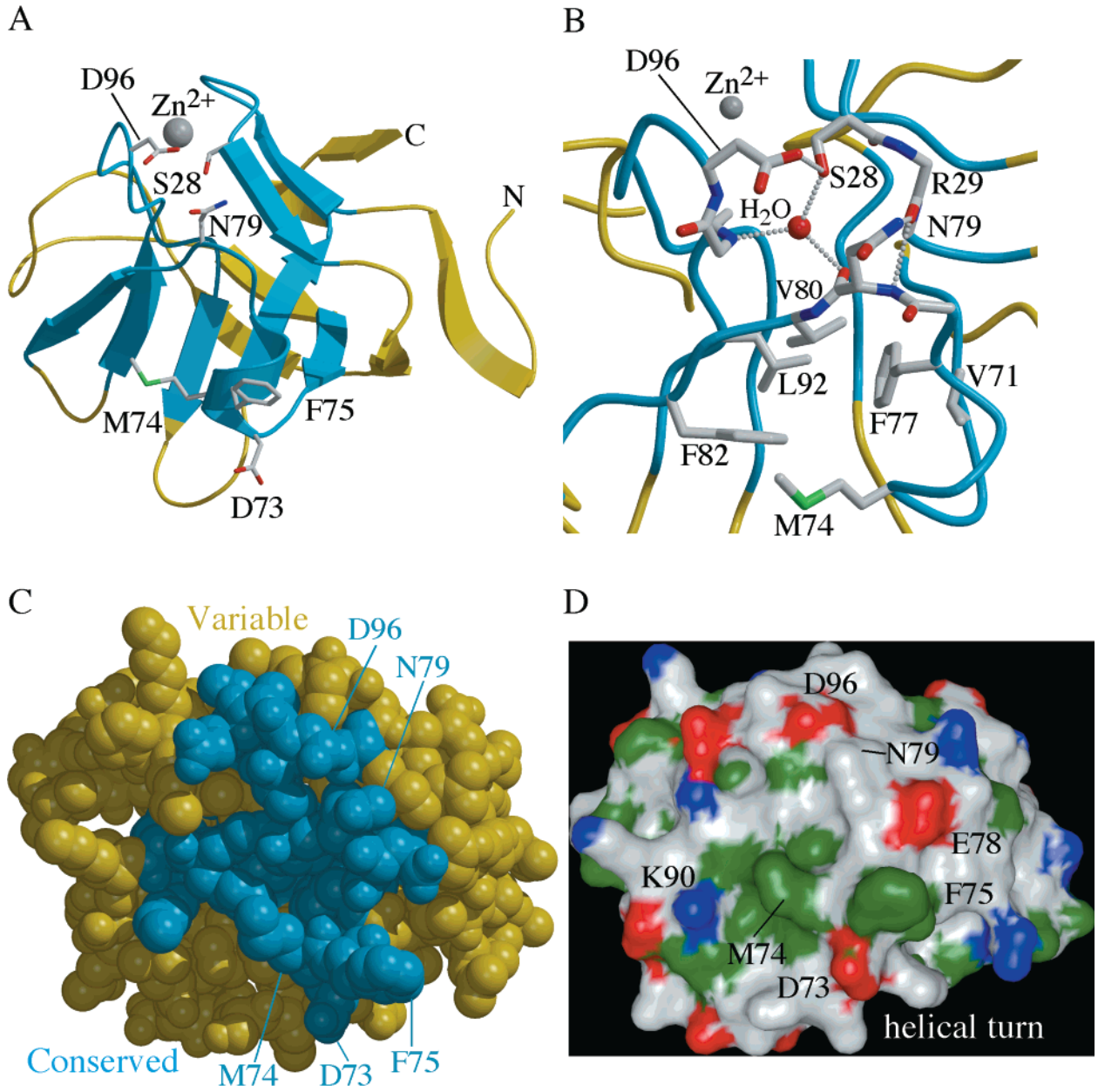

FIGURE 4: Properties of the conserved subdomain. (A) Overall view showing the conserved subdomain (blue) and the location of mutated residues (white). (B) Network of direct and water-mediated interactions that stabilize the Zn^{2+} binding site. (C) Space filling model with the conserved subdomain highlighted in blue. (D) Molecular surface of Mss4 and electrostatic properties of the conserved subdomain. Green represents hydrophobic surface, whereas red and blue regions represent negative potential and positive potential, respectively. The surface potential was contoured in the range from $10k_bT$ to $-10k_bT$, where k_b is Boltzmann's constant and T is the absolute temperature.

the latter variation has been observed in other Zn^{2+} binding proteins (*41*). Consequently, all of the known Mss4 homologues are predicted to bind one Zn^{2+} ion with the thiol groups of cysteine residues from characteristic Zn^{2+} binding motifs serving as ligands.

A Network of Direct and Water-Mediated Intramolecular Interactions Stabilize the Conserved Subdomain. The high-resolution crystal structure of Mss4 reveals a network of direct and water-mediated hydrogen bonding interactions that reinforce the Zn^{2+} binding site and thereby stabilize the hydrophobic core of the conserved subdomain (Figure 4A,B). The same network of intramolecular interactions is observed in both molecules in the asymmetric unit. As shown in Figure 4B, a buried water molecule appears to be important for the integrity of the structure. This water molecule mediates hydrogen bonding interactions with the hydroxyl group of Ser 28, the main chain carbonyl oxygen of Asn 79, and the main chain NH group of Ala 95. In addition, the hydroxyl group of Ser 28 donates a hydrogen bond to the carboxylate group of Asp 96 while the main chain carbonyl oxygen of Arg 29 forms hydrogen bonds with both the side chain and main chain NH group of Asn 79. Although the interactions observed here differ from those in the NMR model (*29*), the residues that mediate these interactions are highly conserved. Thus, the network of intramolecular stabilizing interactions observed in the crystal structure appears to be a general feature of the Mss4 family. As described below, mutation of Ser 28 confirms the importance of these interactions with respect to the integrity of the Zn^{2+} binding site and overall stability of the protein.

The Conserved Subdomain Contains an Exposed Hydrophobic Surface Flanked by Polar or Charged Residues. The

majority of conserved residues in Mss4 either are buried in the hydrophobic core or participate in the network of intramolecular interactions that stabilize the Zn^{2+} binding site. A striking exception involves the 3_{10}A helical turn encoded by residues ^{73}DMF^{75}. Although the main chain atoms are well-ordered, the side chains of these residues are dramatically exposed and do not participate in intramolecular interactions (Figure 4C,D). A strikingly similar DΦΦ helical turn motif in EF-Ts (residues ^{79}DFV^{81}) plays a critical role in disrupting the Mg^{2+} binding site in EF-Tu (*16*, *42*). Following the 3_{10}A helical turn, the side chains of two invariant hydrophobic residues (Phe 77 and Val 80) insert into the hydrophobic core, solidly anchoring the βG−βH loop, and consequently the 3_{10}A helical turn, as it extends across the central β sheet. The packing of Phe 77 and Val 80 in the hydrophobic core, rather than the surface water-mediated interaction between Asn 79 and Asp 96, appears to be the major factor dictating the conformation and stability of the βG−βH loop. As shown in Figure 4D, the partially exposed side chains of Val 80 and two other invariant hydrophobic residues (Phe 82 and Leu 92) form a shallow hydrophobic pocket adjacent to the exposed hydrophobic side chains of Met 74 and Phe 75 in the 3_{10}A helical turn. Thus, the conserved subdomain of Mss4 contains a substantial, exposed hydrophobic patch surrounded by polar and charged residues (Asp 73, Glu 78, Asn 79, Lys 90, and Asp 96). Interestingly, all but one of the residues implicated in the interaction with Rab GTPases by chemical shift perturbations (*29*) and mutation map to this highly conserved surface (see Figures 3, 4C, and 5).

Structural versus Functional Roles of Ser 28, Asn 79, and Asp 96. To gain further insight regarding the roles of Ser 28, Asn 79, and Asp 96 in the stabilization of the conserved subdomain and/or the interaction with Rab GTPases, each of these residues was independently substituted with alanine and the mutant proteins were characterized with respect to nucleotide release activity toward Rab3A (Figure 5A,C) as well as resistance to proteolysis by LysC and ArgC (Figure 6). A detailed kinetic analysis indicates that both Asp 96 and Asn 79 have significant effects on the ability of Mss4 to catalyze nucleotide release; however, the D96A mutant exhibits a more severe defect, reducing the catalytic efficiency (k_{cat}/K_m) by roughly 28-fold (Figure 5C and Table 2). In contrast, the S28A substitution resulted in relatively minor (<3-fold) effects on the apparent catalytic constants. The detailed kinetic analyses presented here for the D96A and N79A mutants are consistent with the results of previous studies in which the nucleotide exchange activity of two related mutants (D96H and N79D) were examined (*28*, *29*).

All of the Mss4 mutants described in this study were expressed in soluble form at wild type levels. Curiously, however, the S28A mutant eluted from the Ni−NTA−agarose column with a red color that was retained through subsequent purification steps, suggesting that the Zn^{2+} ion had been replaced by Ni^{2+}. Several lines of evidence support this hypothesis. First, inclusion of 1 mM $ZnCl_2$ in the elution buffer completely eliminated the red color. Second, the absorption spectrum for the red form of S28A exhibits a peak in the visible region at 485 nm. Absorption bands in the 400−500 nm range are characteristic of thiol coordination to Ni^{2+}. Finally, Ni^{2+} is known to form tetrahedral complexes with thiol ligands. Consistent with these observations, the

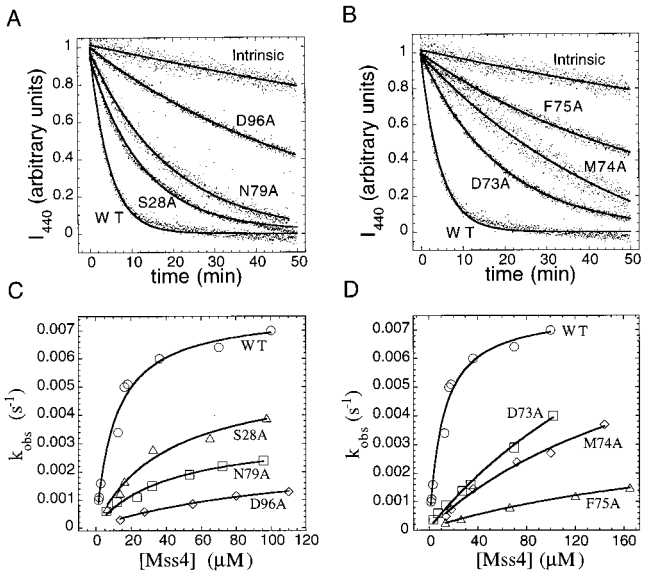

FIGURE 5: Nucleotide release kinetics and catalytic properties of Mss4 mutants. (A and B) Normalized fluorescence time course for the dissociation of MantGDP from Rab3A in the absence (intrinsic) and presence of 13.5 μM wild type (WT) or mutant Mss4 [(A) S28A, N79A, and D96A and (B) D73A, M74A, and F75A]. Solid lines represent the fitted exponential time courses from which pseudo-first-order rate constants were extracted (see Materials and Methods). (C and D) Observed pseudo-first-order rate constants (k_{obs}) as a function of wild type (WT) or mutant Mss4 concentration [(C) S28A, N79A, and D96A and (D) D73A, M74A, and F75A]. Solid lines represent fitted hyperbolic model functions for the dependence of the observed rate constants on the concentration of Mss4 (see Materials and Methods).

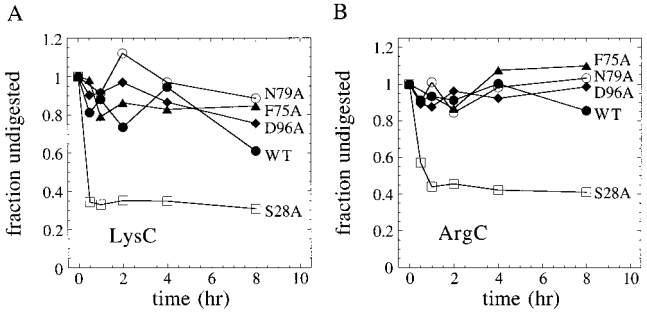

FIGURE 6: Time course for proteolytic digestion of wild type Mss4 (●), S28A (□), F75A (▲), N79A (○), and D96A (◆) by endoproteinase LysC (A) or endoproteinase ArgC (B).

S28A mutant was much more rapidly degraded by both LysC and ArgC, indicating that the structure was significantly destabilized relative to the wild type protein (Figure 6). In sharp contrast, the other mutants (including D96A and N79A) were colorless on elution from the Ni−NTA−agarose column, and those that were examined exhibited proteolysis time courses that were similar to those of the wild type protein.

These data demonstrate that Ser 28 plays an important role with respect to stabilization of the Zn^{2+} binding site but is not a major determinant of the interaction with Rab GTPases. Moreover, loss of the hydrogen bonding interaction between Asp 96 and Ser 28 does not have a detectable effect on the stability of the protein as judged by sensitivity to proteolysis. Nor can it explain the dramatic decrease in catalytic efficiency observed for the D96A substitution, as mutation of Ser 28, which clearly does perturb the structure, has a

relatively modest effect on the ability to catalyze nucleotide release. The simplest explanation is that Asp 96, and likely Asn 79, is conserved primarily for interaction with Rab GTPases or other unidentified proteins, although it is possible that the intramolecular interactions mediated by these residues also contribute to structural stability at a level that is not detected in the proteolysis experiments. The important structural role of Ser 28, on the other hand, is consistent with the network of direct and water-mediated intramolecular interactions observed in the crystal structure (Figure 4B) and explains its evolutionary conservation.

The 3_{10}A Helical Turn Is a Major Determinant of the Interaction with Rab GTPases. To determine whether the EF-Ts-like helical turn motif in Mss4 plays an important role in the nucleotide release mechanism, alanine mutations were independently introduced at Asp 73, Met 74, and Phe 75. The proteolysis patterns for the F75A mutant were indistinguishable from those of wild type Mss4, indicating that the structural integrity remains intact. As shown in Figure 5, the D73A and M74A mutations increased K_m significantly (>10-fold) but had little effect on k_{cat}, suggesting that these residues contribute to the affinity for Rab GTPases but do not participate directly in the rate-limiting step of the nucleotide release reaction. The F75A substitution resulted in a more severe defect, reducing k_{cat}/K_m by ~43-fold. Thus, the F75A and D96A mutations have similarly dramatic effects on the kinetics of nucleotide release (Figure 5 and Table 2). Although the large magnitude of the defects resulting from these substitutions prevents accurate estimation of the apparent catalytic constants, lower and upper limits can be placed on the values of k_{cat} and K_m, respectively (see Table 2). Interestingly, neither mutant is catalytically dead. In fact, any decrease in apparent k_{cat} must be less than 4-fold. As the majority of the defect resides with the apparent K_m, it appears that Phe 75 and Asp 96, like the other conserved residues which have been mutated, contribute more significantly to the interaction with Rab3A than to the rate-limiting step of the catalytic mechanism. Interpreted in the context of the crystal structure and proteolysis experiments, the kinetic characterization of Mss4 mutants provides a partial functional map of the Rab interaction determinants with respect to the conserved subdomain (Figure 7). Five of the six residues examined in this study contribute significantly to the interaction with Rab3A. Moreover, the most dramatic effects are observed for mutation of residues at distal ends of the conserved Rab interaction surface.

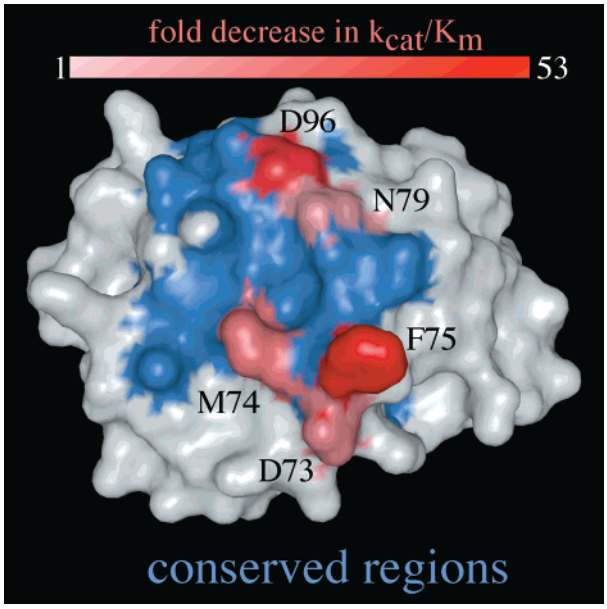

FIGURE 7: Structural and functional correlation of Mss4 mutants. The conserved surface of Mss4 is highlighted in blue, and the fold decrease in catalytic efficiency (k_{cat}/K_m) resulting from alanine substitution is indicated from small (light red) to large (dark red) effects.

DISCUSSION

Mss4 and its yeast homologue Dss4 require Zn^{2+} for stability and have been shown to catalyze nucleotide release for exocytic Rab GTPases in vitro (*23*, *24*, *27*, *43*, *44*). Overexpression of either protein in *Saccharomyces cerevisiae* suppresses the lethal phenotype of dominant negative Sec4 alleles by binding tightly to and thereby sequestering the dominant negative Sec4 mutants (*23*). Microinjection of Mss4 into squid giant axons markedly stimulates neurotransmitter release (*25*), suggesting that Mss4 can function as a GEF for Rab3A in neurons, albeit at levels that exceed those of the endogenous protein. Finally, overexpression of Mss4 in human tumors suggests that it may also play an aberrant role in promoting cell proliferation (*26*), perhaps by enhancing secretion of factors that promote tumor growth. Unlike Sec4, however, Dss4 is not an essential gene for growth under normal conditions (*23*). Likewise, immunodepletion of Mss4 from rat liver cytosol does not disrupt Rab1A-dependent ER to Golgi trafficking (*44*). Clearly, Mss4 proteins cannot be the only GEFs acting on exocytic Rab GTPases. Moreover, the putative upstream signals and/or accessory factors that might activate Mss4 (e.g., by recruitment to vesicle membranes) remain to be determined.

In contrast to the high degree of structural conservation in the GTPase superfamily, GEFs exhibit little homology in either primary or tertiary structure. Nevertheless, all known GEFs bind with high affinity to the nucleotide free form, a critical but unstable intermediate in the exchange reaction. Indeed, the nucleotide free from of Ras is prone to aggregation and possesses properties characteristic of early folding intermediates (*45*−*47*). By binding tightly to and stabilizing the nucleotide free form of exocytic Rab GTPases, Mss4 appears to function by a mechanism similar to that of other GEFs, which promote folded states and can thus be regarded as molecular chaperones. Likewise, Mss4 possesses an apparent K_m for nucleotide release of 11 μM, a value consistent with other GEF-catalyzed exchange reactions assessed in solution (*48*, *49*). Despite the high affinity for the nucleotide free form of exocytic Rab GTPases, the apparent k_{cat} of 0.008 s^{-1} for Mss4-stimulated nucleotide release is low compared to other well-characterized GEFs. These observations are consistent with the hypothesis that Mss4 functions as a molecular chaperone for the intrinsically unstable nucleotide free form of exocytic Rab GTPases (*44*).

In addition to Dss4 from the budding yeast *S. cerevisiae* and mammalian Mss4, a database search revealed ESTs corresponding to five new Mss4 homologues from diverse organisms, including the fission yeast *Saccharomyces pombe*, insects (*Caenorhabditis elegans*, *Drosophila melanogastar*, and *Bombyx mori*), and zebrafish. Aside from the invariant CX_nC motifs required for Zn^{2+} binding, the most striking

features of these sequences are the conservation of residues required to form the core subdomain as well as the residues implicated in the interaction with Rab GTPases. Strict conservation of the Rab interaction epitope within the context of an otherwise hypervariable surface strongly supports a common function for members of the Mss4 family as exocytic Rab GEFs. Moreover, the presence of Mss4 in diverse organisms implies an evolutionary pressure to maintain the gene.

Genetic and biochemical experiments on a number of different GEF−GTPase systems have identified conserved acidic residues that play a key role in the exchange mechanism. Although the specific interactions observed in crystallographic studies of the EF-Ts−EF-Tu, Sos−Ras, and Sec7−Arf1 complexes are quite different, in each case the conserved acidic residues contribute either directly or indirectly to destabilization of the Mg^{2+} binding site (*16*−*18*, *42*). Conserved hydrophobic residues also play a central but apparently distinct role in each of these complexes. In this study, we have identified a conserved serine residue (Ser 28) that is critical for the stability of the Zn^{2+} binding site in Mss4 yet contributes only moderately to nucleotide release activity. Two other conserved residues (Asn 79 and Asp 96) mediate intramolecular hydrogen bonding interactions that would appear to reinforce the Zn^{2+} binding site. Alanine mutants of Asp 96 and (to a lesser extent) Asn 79 show large effects on the kinetics of nucleotide release but exhibit no obvious defect with respect to Zn^{2+} binding or overall stability. The simplest explanation is that Asp 96 and Asn 79 contribute directly to the interaction with Rab GTPases, independent of any potential contribution to structural stability.

Does the interaction of Mss4 with exocytic Rab GTPases reflect a structural mechanism similar to that utilized by EF-Ts to disrupt the Mg^{2+} binding site in EF-Tu? In the crystal structure of the EF-Ts−EF-Tu complex, the Mg^{2+} binding site is disrupted by a 3_{10} helical turn (residues ^{80}DFV^{82}) (*16*). Interestingly, Mss4 possesses a strikingly similar 3_{10} helical turn motif (residues ^{73}DMF^{75}) consisting of an invariant aspartic acid residue followed by two conserved hydrophobic residues. Like their counterparts in EF-Ts, the side chains of all three residues are prominently exposed in the Mss4 structure. Mutation of any of these residues, and in particular Phe 75, severely impairs exchange activity, indicating that the 3_{10}A helical turn in Mss4 is a critical determinant of nucleotide release activity. However, two observations suggest that the specific interactions mediated by the helical turn in Mss4 are likely to differ from those of EF-Ts. First, the main chain $\Phi-\Psi$ angles for Asp 73 in Mss4 differ markedly from those of Asp 80 in EF-Ts such that the relative spatial disposition of the aspartate and hydrophobic side chains in the two DΦΦ motifs is not preserved. Second, modeling experiments indicate that an EF-Ts-like orientation of the helical turn in Mss4 would place Asp 96 near the variable $\alpha3-\beta5$ and $\alpha4-\beta6$ loops of Rab3A, which lie outside the N-terminal third of Rab3A previously implicated in the interaction with Mss4 (*28*). Thus, it appears unlikely that Mss4 and EF-Ts operate by strictly analogous structural mechanisms. Whether the 3_{10}A helical turn in Mss4 directly disrupts the Mg^{2+} binding site in Rab GTPases remains to be determined. Indeed, the chemical functionality and relative spatial disposition of Asn 79 and Asp 96 resemble conserved glutamine and glutamate residues in the Gea1 Sec7 domain that have been shown to disrupt the Mg^{2+} binding site of Arf1 (*18*). Thus, a definitive answer to this question will require the structure of an Mss4−Rab complex.

The crystallographic and mutational data presented here identify key determinants of structural stability and Rab nucleotide release activity within the Mss4 family. The primary hydrophobic core, Zn^{2+} binding site, and Rab interaction epitope reside within an evolutionarily conserved subdomain encoded by four nonconsecutive sequence elements. The conserved Ser 28 anchors a network of direct and water-mediated interactions that reinforce the Zn^{2+} binding site and are essential for the overall stability of the protein. In contrast, intramolecular hydrogen bonding interactions mediated by Asn 79 and Asp 96 contribute moderately (if at all) to structural integrity; however, both residues contribute significantly to the release of nucleotide from Rab3A and thus appear to be conserved primarily for intermolecular interactions, presumably with exocytic Rab GTPases. A strictly conserved DΦΦ motif, corresponding to the first of two helical turns in Mss4, is also a critical Rab interaction determinant. These observations are consistent with a concerted structural mechanism in which distal elements of the conserved structural subdomain cooperatively promote GDP release.

ACKNOWLEDGMENT

We are grateful to Drs. Stuart Schreiber and Hongtao Yu for providing the coordinates of the averaged NMR model for human Mss4 and to Dr. Pietro De Camilli for comments on the manuscript.

REFERENCES

1. Pfeffer, S. R. (1994) *Curr. Opin. Cell Biol. 6*, 522−526.
2. Novick, P., and Zerial, M. (1997) *Curr. Opin. Cell Biol. 9*, 496−504.
3. Olkkonen, V. M., and Stenmark, H. (1997) *Int. Rev. Cytol. 176*, 1−85.
4. Lai, C. C., Boguski, M., Broek, D., and Powers, S. (1993) *Mol. Cell. Biol. 13*, 1345−1352.
5. Boguski, M. S., and McCormick, F. (1993) *Nature 366*, 643−654.
6. Trahey, M., and McCormick, F. (1987) *Science 238*, 542−545.
7. Scheffzek, K., Ahmadian, M. R., and Wittinghofer, A. (1998) *Trends Biochem. Sci. 23*, 257−262.
8. Pai, E. F., Krengel, U., Petsko, G. A., Goody, R. S., Kabsch, W., and Wittinghofer, A. (1990) *EMBO J. 9*, 2351−2359.
9. Noel, J. P., Hamm, H. E., and Sigler, P. B. (1993) *Nature 366*, 654−663.
10. Coleman, D. E., Berghuis, A. M., Lee, E., Linder, M. E., Gilman, A. G., and Sprang, S. R. (1994) *Science 265*, 1405−1412.
11. Scheffzek, K., Klebe, C., Fritz-Wolf, K., Kabsch, W., and Wittinghofer, A. (1995) *Nature 374*, 378−381.
12. Hirshberg, M., Stockley, R. W., Dodson, G., and Webb, M. R. (1997) *Nat. Struct. Biol. 4*, 147−152.
13. Jurnak, F. (1985) *Science 230*, 32−36.
14. Greasley, S. E., Jhoti, H., Teahan, C., Solari, R., Fensome, A., Thomas, G. M., Cockcroft, S., and Bax, B. (1995) *Nat. Struct. Biol. 2*, 797−806.
15. Ihara, K., Muraguchi, S., Kato, M., Shimizu, T., Shirakawa, M., Kuroda, S., Kaibuchi, K., and Hakoshima, T. (1998) *J. Biol. Chem. 273*, 9656−9666.
16. Kawashima, T., Berthet-Colominas, C., Wulff, M., Cusack, S., and Leberman, R. (1996) *Nature 379*, 511−518.

17. Boriack-Sjodin, P. A., Margarit, S. M., Bar-Sagi, D., and Kuriyan, J. (1998) *Nature 394*, 337−343.
18. Goldberg, J. (1998) *Cell 95*, 237−248.
19. Wada, M., Nakanishi, H., Satoh, A., Hirano, H., Obaishi, H., Matsuura, Y., and Takai, Y. (1997) *J. Biol. Chem. 272*, 3875−3878.
20. Hama, H., Tall, G. G., and Horazdovsky, B. F. (1999) *J. Biol. Chem. 274*, 15284−15291.
21. Rosa, J. L., Casaroli-Marano, R. P., Buckler, A. J., Vilaro, S., and Barbacid, M. (1996) *EMBO J. 15*, 4262−4273.
22. Horiuchi, H., Lippe, R., McBride, H. M., Rubino, M., Woodman, P., Stenmark, H., Rybin, V., Wilm, M., Ashman, K., Mann, M., and Zerial, M. (1997) *Cell 90*, 1149−1159.
23. Moya, M., Roberts, D., and Novick, P. (1993) *Nature 361*, 460−463.
24. Burton, J., Roberts, D., Montaldi, M., Novick, P., and De Camilli, P. (1993) *Nature 361*, 464−467.
25. Burton, J. L., Burns, M. E., Gatti, E., Augustine, G. J., and De Camilli, P. (1994) *EMBO J. 13*, 5547−5558.
26. Muller-Pillasch, F., Zimmerhackl, F., Lacher, U., Schultz, N., Hameister, H., Varga, G., Friess, H., Buchler, M., Adler, G., and Gress, T. M. (1997) *Genomics 46*, 389−396.
27. Yu, H., and Schreiber, S. L. (1995) *Biochemistry 34*, 9103−9110.
28. Burton, J. L., Slepnev, V., and De Camilli, P. V. (1997) *J. Biol. Chem. 272*, 3663−3668.
29. Yu, H., and Schreiber, S. L. (1995) *Nature 376*, 788−791.
30. Otwinowski, Z., and Minor, W. (1994) *Methods Enzymol. 276*, 307−326.
31. Bailey, S. (1994) *Acta Crystallogr. D50*, 760−763.
32. Brunger, A. T. (1992) *X-plor Version 3.1. A System for X-ray Crystallography and NMR*, Yale University Press, New Haven, CT.
33. Jones, T. A., Zou, J. Y., Cowan, S. W., and Kjeldgaard, M. (1991) *Acta Crystallogr. A47*, 110−119.
34. Kraulis, P. J. (1991) *J. Appl. Crystallogr. 24*, 946−950.
35. Nicholls, A., Bharadwaj, R., and Honig, B. (1993) *Biophys. J. 64*, A166.
36. Merritt, E. A., and Bacon, D. J. (1997) *Methods Enzymol. 277*, 505−524.
37. Hiratsuka, T. (1983) *Biochim. Biophys. Acta 742*, 496−508.
38. Press, W. H., Flannery, B. P., Teukolsky, S. A., and Vetterling, W. T. (1986) *Numerical Recipes*, Cambridge University Press, Cambridge, U.K.
39. Altschul, S. F., Madden, T. L., Schaffer, A. A., Zhang, J., Zhang, Z., Miller, W., and Lipman, D. J. (1997) *Nucleic Acids Res. 25*, 3389−3402.
40. Altschul, S. F., Gish, W., Miller, W., Myers, E. W., and Lipman, D. J. (1990) *J. Mol. Biol. 215*, 403−410.
41. Schwabe, J. W., and Klug, A. (1994) *Nat. Struct. Biol. 1*, 345−349.
42. Zhang, Y., Li, X., and Spremulli, L. L. (1996) *FEBS Lett. 391*, 330−332.
43. Collins, R. N., Brennwald, P., Garrett, M., Lauring, A., and Novick, P. (1997) *J. Biol. Chem. 272*, 18281−18289.
44. Nuoffer, C., Wu, S. K., Dascher, C., and Balch, W. E. (1997) *Mol. Biol. Cell 8*, 1305−1316.
45. Zhang, J., and Matthews, C. R. (1998) *Biochemistry 37*, 14891−14899.
46. Zhang, J., and Matthews, C. R. (1998) *Biochemistry 37*, 14881−14890.
47. Feuerstein, J., Goody, R. S., and Wittinghofer, A. (1987) *J. Biol. Chem. 262*, 8455−8458.
48. Beraud-Dufour, S., Robineau, S., Chardin, P., Paris, S., Chabre, M., Cherfils, J., and Antonny, B. (1998) *EMBO J. 17*, 3651−3659.
49. Lenzen, C., Cool, R. H., Prinz, H., Kuhlmann, J., and Wittinghofer, A. (1998) *Biochemistry 37*, 7420−7430.

BI002680O